of the culmen (0.1 mm)[10]. Measurements were averaged within species. Altogether, the data set comprised 1,018 (17.8% of 5,712) species in 103 (97.2% of 106) suprageneric taxa of passerine birds.

Two samples of tribe-to-family-level clades were analysed. The most inclusive contained the 95 taxa for which I measured more than one species and could therefore calculate morphological variance. The second sample ($n = 50$) excluded clades restricted to non-continental landmasses (primarily Australasia, New Zealand, Madagascar and the Greater Antilles), as well as tribe-to-family-level clades for which I measured fewer species than one-third the number of genera or one-tenth the number of species.

In a further analysis, I extended the range of clade age by including estimates of morphological variance within 108 genera having five or more species and for which I had measured more than 20% of all species. Genera were assigned a relative age of $\Delta T_{50}H = 3.2$ °C (the median relative age of nodes within subtribes)[24]. These were combined with well-sampled tribe-to-family-level clades.

Sympatry within small clades

I used distribution maps in field guides and handbooks to estimate by eye the approximate degree of sympatry among the species in clades having fewer than ten species (see Supplementary Table 2). For each clade, the sympatry index is the proportion of species (0–1) having greater than ≈50% overlap in their geographic range with one or more other species in the clade, hence having the potential for interacting locally.

Analyses

The eight morphological values were $\log_{10}$-transformed to make the distribution of variation in each of the measurements dimensionless, approximately normal within the sample of species and unrelated to the mean value of the measurement. Over all species, standard deviations of the log-transformed measurements varied between 0.144 and 0.195 (equivalent to factors of 1.39 and 1.57) and thus large and small measurements contributed comparably to distance between species in morphological space. Log-transformed measurements were subjected to a principal components (PC) analysis based on the covariance matrix, to reduce the dimensionality of the data and obtain uncorrelated axes of morphological variation. Using the covariance matrix preserves the original euclidean distances between species[26].

The first PC axis incorporated 75% of the variance in morphology and the first three axes incorporated 91%. The resulting eight PC scores for each species were then used to estimate the variance on each of the PC axes for each tribe-to-family-level clade. The estimate of the variance is unbiased with respect to sample size[1]. Among 95 clades, the morphological standard deviation was phylogenetically independent according to Abouheif's test[25] for PC1 ($P = 0.55$) and PC4 ($P = 0.17$).

To test the hypothesis that morphological diversification is a function of number of species, time or both, I used multiple regression to determine the relationship between morphological variance on each of the PC axes and the logarithm of species number and relative age of each clade. Each of the variables was log-transformed to make the deviations of morphological variance about the regression uniform and to test the linearity of the relationship (slope = 1).

I conducted nested analyses of variance to examine the distribution of variation among species within genera, genera within tribe-to-family-level clades, and clades within passerines. The expected morphological variation depending on a direct relationship to the logarithm of species was calculated as follows: the logarithm of the number of smaller taxa within each larger taxon at each level in the hierarchy of analysis (that is, 106 clades within passerines, 10.95 genera per clade and 4.92 species per genus).

All analyses were performed using the Statistical Analysis System (SAS Institute, Cary, North Carolina).

Received 3 November 2003; accepted 24 May 2004; doi:10.1038/nature02700.

1. Foote, M. The evolution of morphological diversity. *Annu. Rev. Ecol. Syst.* **28,** 129–152 (1997).
2. Harmon, L. J., Schulte, J. A. II, Larson, A. & Losos, J. B. Tempo and mode of evolutionary radiation in iguanian lizards. *Science* **301,** 961–964 (2003).
3. Simpson, G. G. *The Major Features of Evolution* (Columbia Univ. Press, New York, 1953).
4. Gould, S. J. & Eldredge, N. Punctuated equilibria: the tempo and mode of evolution reconsidered. *Paleobiology* **3,** 115–151 (1977).
5. Jackson, J. B. C. & Cheetham, A. H. Tempo and mode of speciation in the sea. *Trends Ecol. Evol.* **14,** 72–77 (1999).
6. Raup, D. M. & Gould, S. J. Stochastic simulation and evolution of morphology–towards a nomothetic paleontology. *Syst. Zool.* **23,** 305–322 (1974).
7. Foote, M. in *Evolutionary Paleobiology* (eds Jablonski, D., Erwin, D. H. & Lipps, J. H.) 62–86 (Univ. Chicago Press, Chicago, 1996).
8. Miles, D. B. & Ricklefs, R. E. The correlation between ecology and morphology in deciduous forest passerine birds. *Ecology* **65,** 1629–1640 (1984).
9. Ricklefs, R. E. & Miles, D. B. in *Ecological Morphology. Integrative Organismal Biology* (eds Wainwright, P. C. & Reilly, S. M.) 13–41 (Univ. Chicago Press, Chicago, 1994).
10. Ricklefs, R. E. & Travis, J. A morphological approach to the study of avian community organization. *Auk* **97,** 321–338 (1980).
11. Benkman, C. W. Divergent selection drives the adaptive radiation of crossbills. *Evolution* **57,** 1176–1181 (2003).
12. Moritz, C., Patton, J. L., Schneider, C. J. & Smith, T. B. Diversification of rainforest faunas: an integrated molecular approach. *Annu. Rev. Ecol. Syst.* **31,** 533–563 (2000).
13. Schluter, D. Morphological and phylogenetic relations among the Darwin's finches. *Evolution* **38,** 921–930 (1984).
14. Lack, D. *Darwin's Finches* (Cambridge Univ. Press, Cambridge, 1947).
15. Grant, P. R. Convergent and divergent character displacement. *Biol. J. Linn. Soc.* **4,** 39–68 (1972).
16. Schluter, D. Character displacement and the adaptive divergence of finches on islands and continents. *Am. Nat.* **131,** 799–824 (1988).
17. Schluter, D. Ecological causes of adaptive radiation. *Am. Nat.* **148,** S40–S64 (1996).
18. Lovette, I. J., Bermingham, E. & Ricklefs, R. E. Clade-specific morphological diversification and adaptive radiation in Hawaiian songbirds. *Proc. R. Soc. Lond. B* **269,** 37–42 (2002).
19. Schluter, D. *The Ecology of Adaptive Radiation* (Oxford Univ. Press, Oxford, 2000).
20. Ricklefs, R. E. Global diversification rates of passerine birds. *Proc. R. Soc. Lond. B* **270,** 2285–2291 (2003).
21. Eldredge, N. & Gould, S. J. in *Models in Paleobiology* (ed. Schopf, T. J. M.) 82–115 (Freeman, San Francisco, 1972).
22. Carson, H. L. & Templeton, A. R. Genetic revolutions in relation to speciation phenomena: the founding of new populations. *Annu. Rev. Ecol. Syst.* **15,** 97–131 (1984).
23. Sibley, C. G. & Monroe, B. L. Jr. *Distribution and Taxonomy of Birds of the World* (Yale Univ. Press, New Haven, Connecticut, 1990).
24. Sibley, C. G. & Ahlquist, J. E. *Phylogeny and Classification of the Birds of the World* (Yale Univ. Press, New Haven, Connecticut, 1990).
25. Abouheif, E. A method to test the assumption of phylogenetic independence in comparative data. *Evol. Ecol. Res.* **1,** 895–909 (1999).
26. Legendre, P. & Legendre, L. *Numerical Ecology* (Elsevier, Amsterdam, 1998).

Supplementary Information accompanies the paper on **www.nature.com/nature**.

Acknowledgements I thank M. Foote, T. Givnish and S. S. Renner for constructive comments. For access to specimens, I am grateful to curators and collection managers at the Academy of Natural Sciences in Philadelphia, the US National museum, the American Museum of Natural History, the Field Museum in Chicago, the Bavarian State Collections in Munich, the Senckenberg Museum in Frankfurt and the Museum des Sciences Naturelles in Brussels. This work was supported in part by research funds available to Curators' Professors at the University of Missouri.

Competing interests statement The authors declare that they have no competing financial interests.

Correspondence and requests for materials should be addressed to R.E.R. (ricklefs@umsl.edu).

The combined effects of pathogens and predators on insect outbreaks

Greg Dwyer[1], Jonathan Dushoff[2] & Susan Harrell Yee[1]

[1]*Department of Ecology and Evolution, 1101 E 57th Street, University of Chicago, Chicago, Illinois 60637-1573, USA*
[2]*Department of Ecology and Evolutionary Biology, Princeton University, Princeton, New Jersey 08544, USA*

The economic damage caused by episodic outbreaks of forest-defoliating insects has spurred much research[1], yet why such outbreaks occur remains unclear[2]. Theoretical biologists argue that outbreaks are driven by specialist pathogens or parasitoids, because host–pathogen and host–parasitoid models show large-amplitude, long-period cycles resembling time series of outbreaks[3,4]. Field biologists counter that outbreaks occur when generalist predators fail, because predation in low-density defoliator populations is usually high enough to prevent outbreaks[5–8]. Neither explanation is sufficient, however, because the time between outbreaks in the data is far more variable than in host–pathogen and host–parasitoid models[1,2], and far shorter than in generalist-predator models[9–11]. Here we show that insect outbreaks can be explained by a model that includes both a generalist predator and a specialist pathogen. In this host–pathogen–predator model, stochasticity causes defoliator densities to fluctuate erratically between an equilibrium maintained by the predator, and cycles driven by the pathogen[12,13]. Outbreaks in this model occur at long but irregular intervals, matching the data. Our results suggest that explanations of insect outbreaks must go beyond classical models to consider interactions among multiple species.

The host–pathogen model that we begin with describes the effects of a specialist pathogen on the population dynamics of a forest defoliator. Host-specific pathogens of defoliators are often baculoviruses, which cause fatal diseases transmitted when larvae

consume foliage contaminated with infectious cadavers[14]. Although baculoviruses infect only larvae, multiple rounds of transmission within a generation can lead to high infection rates, and so epidemics are often severe in high-density defoliator populations[1,15,16]. Infected larvae are converted into infectious cadavers, and pathogens are reintroduced into defoliator populations the following year when hatchlings encounter infectious particles from the previous year[17]. Previous work has shown that these dynamics can be accurately predicted by a standard epidemic model, modified to allow for variability in susceptibility among hosts[18]. The fraction of infected hosts, I, in such a model can be closely approximated by the following implicit expression, derived by assuming that the epidemic proceeds until no further infections occur[19]:

$$1 - I(N_t, Z_t) = \left(1 + \frac{\bar{\nu}}{\mu k}(N_t I(N_t, Z_t) + \rho Z_t)\right)^{-k} \quad (1)$$

Here N_t and Z_t are host and pathogen densities in generation t, μ is the rate at which cadavers lose infectiousness, and ρ is the susceptibility of hatchlings relative to later-stage larvae. To allow for variability in susceptibility among larvae, transmission rates in the model follow a gamma distribution with average transmission $\bar{\nu}$ and inverse squared coefficient of variation k. Because most outbreaking defoliators have only one generation per year[20], generations are discrete. Between model generations, surviving defoliators lay eggs, and virus particles must survive in the environment until new host larvae hatch. The host–pathogen model is therefore

$$N_{t+1} = \lambda N_t (1 - I(N_t, Z_t)) \quad (2)$$

$$Z_{t+1} = f N_t I(N_t, Z_t) \quad (3)$$

Here λ is net defoliator fecundity, f is pathogen over-winter survival, and I is calculated using equation (1). For realistic parameter values, this model shows long-period, large-amplitude cycles in defoliator densities[19]. The period and amplitude of these cycles are similar to those seen in time series for many outbreaking insects[19], except that the cycle period is much more regular in the model than in the data. To see whether this discrepancy could be explained through the addition of stochasticity, we multiplied the right-hand side of equation (2) by a log-normally distributed random variable ε_t, with median 1. The model cycles, however, are so robust that stochasticity has only a modest effect (Fig. 1a).

We therefore modified the model to allow for a generalist predator, because low-density defoliator populations often experience severe mortality from generalists such as birds[7], spiders[5], small mammals[6] or generalist parasitoids[8,21]. Generalists by definition rely on multiple resources, and so, in contrast to specialists, their densities respond weakly or not at all to changes in prey density. A generalist's attack rate can nevertheless respond to density, if, for example, the generalist switches among prey items according to the relative availability of each item[22]. Allowing for such behaviour

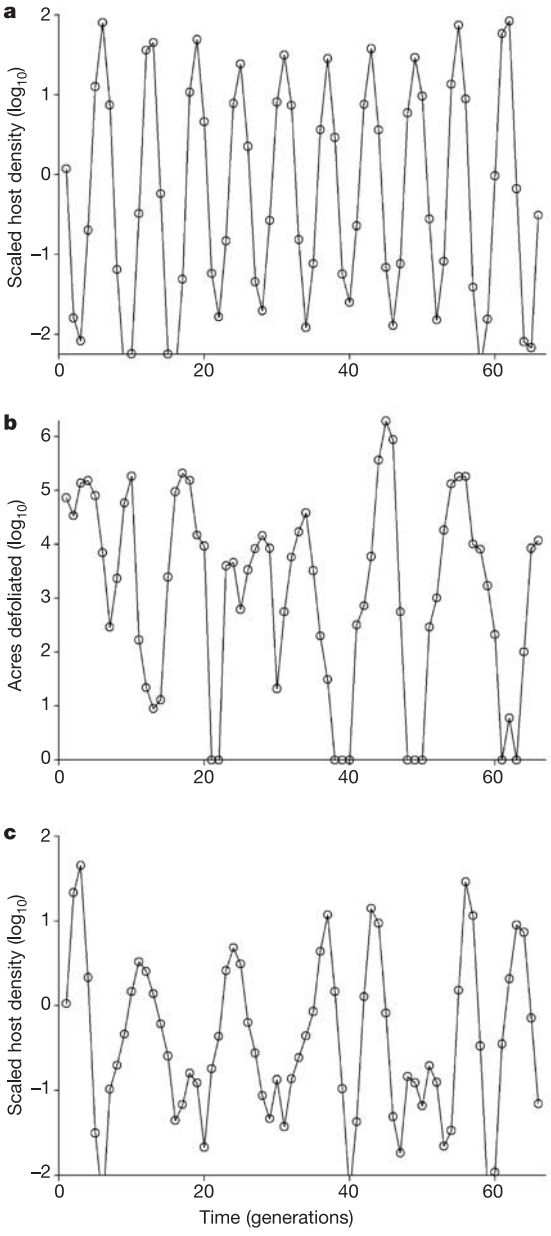

Figure 1 Comparison of model output with data for an outbreaking insect. **a**, Host–pathogen model, equations (1)–(3). **b**, Gypsy moth defoliation in New Hampshire, USA. **c**, Combined model, equations (1), (4) and (5). Parameter values are in the Methods, with the addition that the standard deviation of $\log_e$ of the forcing term ε_t is 0.5. Model output is scaled as described in the Methods. Note that the data give areas defoliated, whereas the models give densities, so in comparing models with data we focus on the time between outbreaks rather than on outbreak amplitudes.

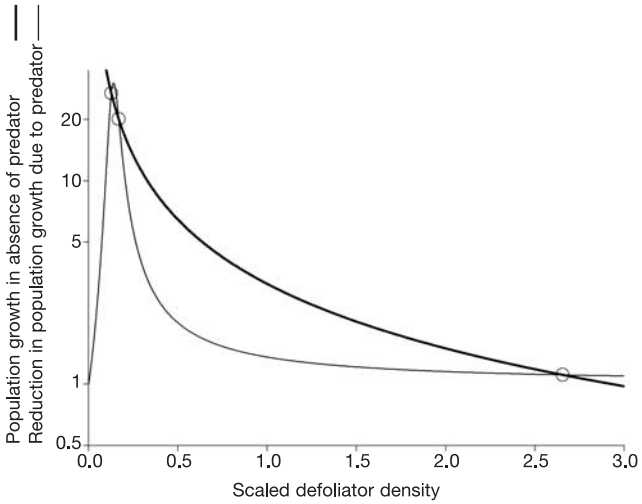

Figure 2 Graphical representation of the combined model's equilibria. The dark line is the defoliator's quasi-equilibrium population growth in the absence of the predator, and the light line is the relative reduction in the defoliator growth rate due to the predator. Circled intersections are equilibria.

produces the model:

$$N_{t+1} = \lambda N_t(1 - I(N_t, Z_t))\left(1 - \frac{2abN_t}{b^2 + N_t^2}\right) \quad (4)$$

$$Z_{t+1} = fN_t I(N_t, Z_t) \quad (5)$$

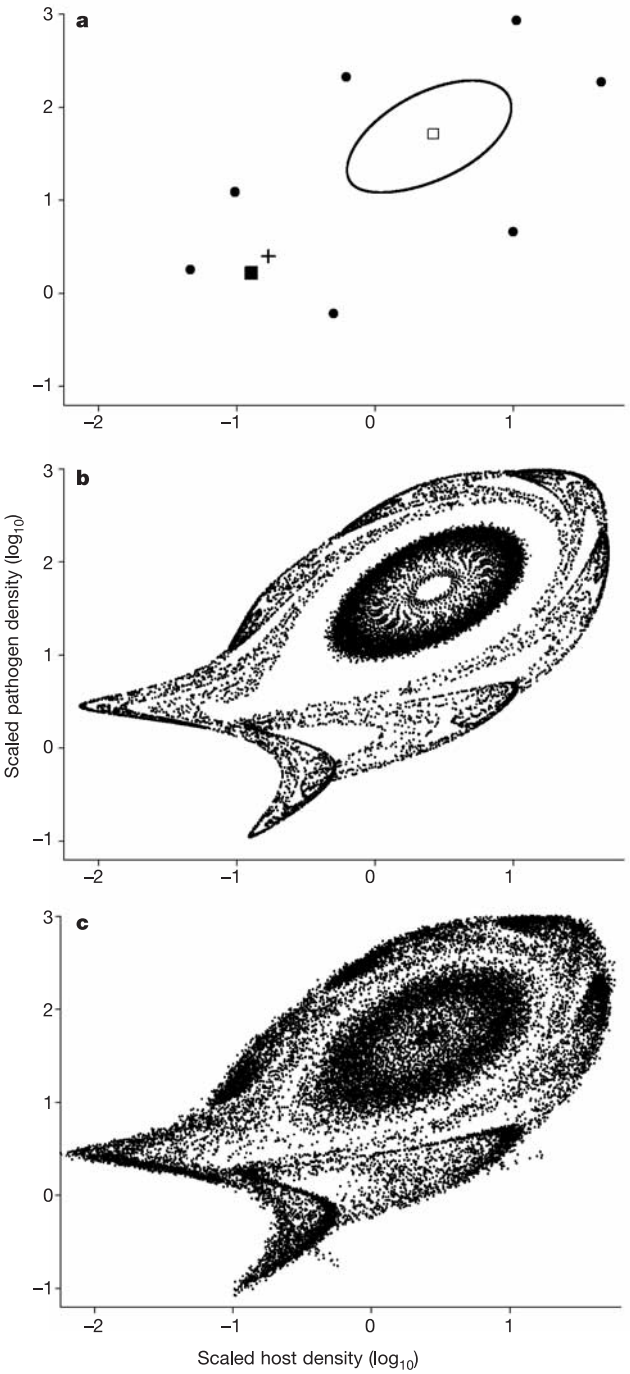

Figure 3 Phase portraits of the combined model, with time proceeding anticlockwise. **a**, Deterministic attractors. The ellipse is a quasi-periodic attractor and the small circles are a phase-locked limit cycle. Source, sink and saddle-point equilibria are depicted by an open square, a closed square and a cross, respectively. **b**, Short-term dynamics for many initial conditions. We iterated the model for 250 generations, discarded the first 150 generations, plotted values for the remaining generations[12], and repeated for initial N_t from 0.001 to 500 and initial Z_t from 0.01 to 10,000, multiplying by 1.4 at each step. **c**, Long-term dynamics with stochasticity. The standard deviation of the $\log_e$ of the forcing term is 0.05. Note that, unlike in **b**, densities never settle on a single attractor.

Here the fraction of defoliators killed by the predator is $2abN_t/(b^2 + N_t^2)$, where a is the maximum fraction killed, and b is the defoliator density at which the fraction killed is maximized. Note that the fraction killed by the predator rises rapidly with increasing prey density as the predator specializes on the newly abundant prey. At high densities, however, the predator is overwhelmed, and the attack rate levels off. The reduction in the defoliator's population growth rate due to the predator is therefore maximized at an intermediate density (Fig. 2). Generalist predators usually have little impact at high density, but often impose density-dependent regulation on low-density defoliator populations[5–8,21], consistent with this model.

The addition of the generalist predator leads to dynamics that are much more complex than the dynamics of the host–pathogen model. This dynamical complexity arises in part because the combined model can have multiple equilibria. To find these equilibria, we consider a quasi-equilibrium[11] at which pathogen density instantaneously adjusts to host density. At this quasi-equilibrium, we can calculate the defoliator's population growth rate as a function of defoliator density alone (Fig. 2). Model equilibria then occur at densities for which the quasi-equilibrium population growth rate in the absence of the predator is equal to the reduction due to the predator (Fig. 2). The model can have multiple equilibria because the reduction due to the predator reaches a maximum at an intermediate density.

Our results hold for a wide range of parameter values (see Supplementary Information), but to describe the model's dynamics in more detail, we use values calculated for the gypsy moth (*Lymantria dispar*) in North America (for data sources see the Methods). For these values, the combined model has a high-density equilibrium at which the defoliator is controlled by the pathogen and the predator is relatively unimportant, much as in the host–pathogen model (Fig. 2). In contrast to the host–pathogen model, however, there is also a low-density equilibrium at which these roles are reversed, so that the predator controls the defoliator and the pathogen is relatively unimportant. This predator-maintained equilibrium is stable, but only locally, and the equilibrium coexists with two attractors associated with the high-density equilibrium (Fig. 3a). The long-term model dynamics therefore depend on the initial densities of defoliators and pathogens; moreover, many initial conditions lead to complex transient dynamics that can last many generations[12] (Fig. 3b). The occurrence of multiple attractors and long transients in turn means that adding a small amount of stochasticity—by multiplying the right-hand side of equation (4) by the log-normal random variable ε_t—causes trajectories to move unpredictably among attractors[13] (Fig. 3c). For slightly different parameter values the low-density equilibrium becomes unstable and the system exhibits deterministic chaos. These chaotic dynamics are qualitatively similar to the stochastically induced complex dynamics shown in Fig. 3c.

This dynamical complexity is important because it can help to explain the high levels of variability in outbreak interval seen in

Table 1 **Analysis of time between outbreaks for some forest-defoliating insects**

Species	Location	Average period (yr)	Coefficient of variation of period
Bupalus piniarius[28]	Germany	9.8	0.44
Epirrita autumnata[29]	Finland	9.5	0.26
Lymantria dispar[27]	Maine, USA	9.3	0.19
	Massachusetts, USA	10.5	0.59
	New Hampshire, USA	8.1	0.37
	Vermont, USA	10.0	0.67
Orgyia pseudotsugata[16]	British Columbia, Canada	9.3	0.22
	Washington, USA	13.0	0.62
	N Idaho and NE Oregon, USA	9.0	0.16
	SW Idaho, USA	10.8	0.30
Quadricalcarifera punctatella[30]	Japan	14.6	0.43

most (but not all[2]) long-term defoliator time series (Fig. 1, Table 1). Direct comparison of model output with data is problematic, however, because the model is highly sensitive to initial conditions, and we do not have even crude estimates of the starting densities for any defoliator. One solution is to compare statistical moments of the model output with statistical moments of the data[23], and so we compare the average and the coefficient of variation of the time between outbreaks in the model with those in the data. Figure 4 shows that the combined model yields long average times between outbreaks, and high levels of variability in the time between outbreaks. Although confidence intervals are wide, the mean and the coefficient of variation of the time between outbreaks in the combined model are at least consistent with most of the data. In contrast, although the host–pathogen model—equations (1)–(3)—also shows a long average time between outbreaks, its cycles are very robust, and so achieving similar levels of variability in that model requires very high levels of stochasticity.

Because of the importance of weather in defoliator population dynamics[2], we have assumed that the major source of stochasticity is random fluctuations in parameter values caused by extrinsic events, so-called 'environmental stochasticity'. Although 'demographic stochasticity', the chance events that befall small populations, could conceivably be important in low-density defoliator populations, most such populations are of large spatial extent, and so we suspect that absolute numbers of most defoliators generally do not fall low enough for demographic stochasticity to be of great importance. A related issue is that forest defoliator populations tend to be synchronized over large areas[2], but for some chaotic ecological models, the addition of spatial structure can lead to asynchrony among subpopulations[24]. When we add spatial structure to our model, however, we still see high levels of synchrony among subpopulations (see Supplementary Information). Understanding why our model gives spatial synchrony when other models do not requires additional research, but we suspect that an important part of the explanation is that the long time between outbreaks in our model makes it more difficult for subpopulations to get out of phase with one another. Our results are similarly robust to changes in the specialist natural enemy. If we instead begin with a host–parasitoid model, adding a generalist predator again gives multiple equilibria, and complex dynamics that arise in response to stochasticity (see Supplementary Information).

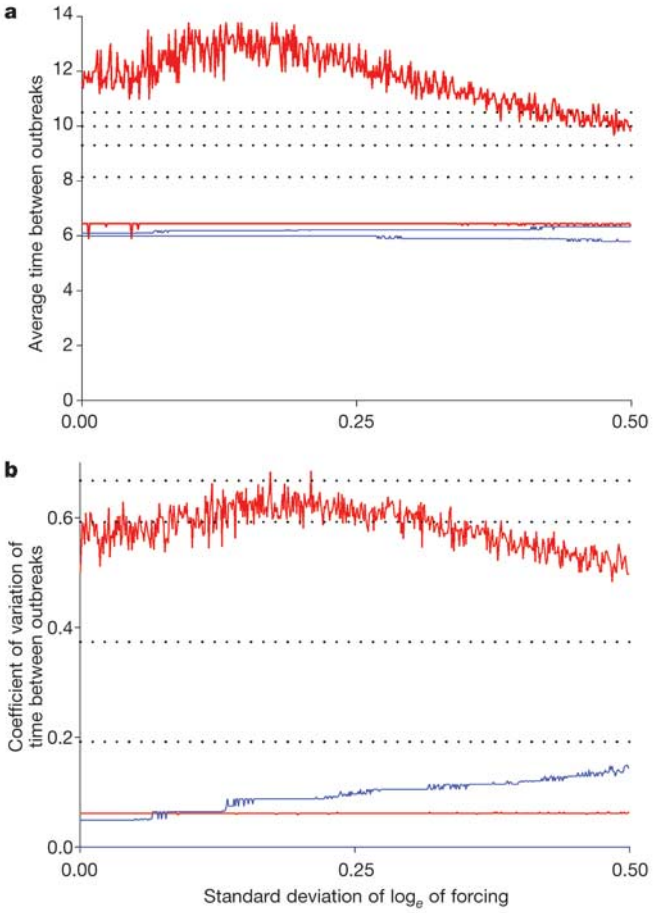

Figure 4 Effects of stochasticity on time between outbreaks. **a**, Average time between outbreaks. **b**, Coefficient of variation of time between outbreaks. We used the models to generate 2,000 realizations of 134 generations each, the approximate number of generations for which the gypsy moth has been resident in North America. We then calculated the average and the coefficient of variation of the time between outbreaks for the final 65 generations, the length of the gypsy moth time series used in Table 1. Initial densities of hosts and pathogens were drawn randomly from a uniform distribution between 0.01 and 100. Lines depict 95th centiles of each statistic. Red lines are for the combined model equations (1), (4) and (5). Blue lines are for the host–pathogen model equations (1)–(3). Dotted lines indicate data for the gypsy moth (Table 1).

Our results show that the addition of a generalist predator to a classical host–pathogen model can create a stable, low-density equilibrium, and that interactions between this equilibrium and limit cycles induced by the pathogen lead to stochastically induced complex dynamics, and thus high variability in the time between insect outbreaks. These dynamics differ not only from those of classical host–pathogen and host–parasitoid models, but also from those of classical generalist-predator models. Although classical generalist-predator models can also have multiple equilibria[9–11], they assume that high-density defoliator populations are kept in check by competition for resources. Outbreaks in these models are separated by decades of low, stable defoliator densities, and so biologists have assumed that outbreaks will only occur when generalist predators fail because of weather or other stochastic factors[1,5–8]. In contrast, because we realistically assume that high-density populations crash owing to a specialist pathogen, the upper equilibrium in our model shows high-amplitude cycles. The stabilizing effect of the generalist predator in our model is therefore much smaller than in classical generalist-predator models. Our work suggests that two-species models are insufficient for understanding outbreaks, whether in insects or in other outbreaking animal taxa[8], and that classical theories of outbreaks must be extended to consider interactions among multiple species. Moreover, models with multiple equilibria are generally used only to describe catastrophic shifts in ecosystems[25]. Our work suggests that an additional important effect of multiple equilibria is the creation of complex dynamics. □

Methods

To reduce the number of parameters, we rewrite the model equations (1), (4) and (5) using the non-dimensionalized host and pathogen densities $\hat{N}_t \equiv \mu N_t/\bar{\nu}$ and $\hat{Z}_t \equiv \mu Z_t/\bar{\nu}$ (ref. 19). This gives the rescaled equations

$$1 - I(N_t, Z_t) = \left(1 + \frac{1}{k}(N_t I(N_t, Z_t) + Z_t)\right)^{-k} \quad (6)$$

$$N_{t+1} = \lambda N_t (1 - I(N_t, Z_t))\left(1 - \frac{2a\hat{b}N_t}{\hat{b}^2 + N_t^2}\right) \quad (7)$$

$$Z_{t+1} = \phi N_t I(N_t, Z_t) \quad (8)$$

where $\hat{b}$ is the ratio of the density at maximum predation b to the epidemic threshold $N_e \equiv \mu/\bar{\nu}$, while ϕ is the between-season impact of the pathogen. At the quasi-equilibrium, pathogen density adjusts to its equilibrium value instantaneously: that is, we set pathogen density Z_t to its equilibrium value $\bar{Z} = \phi N_t I(N_t, \bar{Z})$. This allows us to eliminate Z_t from equation (6), so that equilibria occur at the intersections of the functions $f(N_t) \equiv \lambda(1 - I(N_t))$ and $g(N_t) \equiv 1/[1 - 2a\hat{b}N_t/(\hat{b}^2 + N_t^2)]$.

Our estimates of the transmission parameters $\bar{\nu}$, k and μ are averages from field experiments with the gypsy moth baculovirus[18]. Studies of low-density gypsy moth populations permit estimation of the reproductive rate, λ, independently of density-dependent sources of mortality[6], and provide an estimate of the equilibrium density during non-outbreak years. Although this is not quite the same as b, the density at

maximum predation, the two densities are close relative to the uncertainty in our estimates. These calculations give the following values: $\lambda = 74.6$; $k = 1.06$; $\hat{b} = 0.14$.

Estimates of predation rates in gypsy moth populations often exceed 99% (ref. 21), which for our parameter values gives deterministic chaos in the combined model in the absence of stochasticity. Because these experimental estimates may be slightly inflated relative to predation rates in natural populations[6], in the figures we use the slightly lower value of $a = 0.967$. For $a = 0.967$ and $\phi = 20$, the model has three equilibria, with the lowest one stable (the intermediate-density equilibrium is always unstable), usefully illustrating the origins of complex dynamics in our model. In fact, as we demonstrate in the Supplementary Information, our results hold for a wide range of parameter values. We estimated the pathogen over-winter survival parameter, ϕ, by first estimating the other parameters, and then adjusting ϕ until the amplitude of density fluctuations in each model matched estimates of the amplitude of density fluctuations derived from the literature[26] (note that the data used to estimate ϕ are densities, and are thus unrelated to the areas defoliated in Figs 1 and 4). Deriving an estimate of the density amplitude from the literature requires that we make some assumption about the detection threshold, the lowest density that can be detected. For detection thresholds of 1–2 egg masses per hectare, our amplitude estimates range from 3.38 to 3.68 orders of magnitude. In this range of amplitude estimates, the inherent stochasticity of the combined model makes it difficult to estimate ϕ with more than one significant digit. Given these uncertainties, we take 3.5 orders of magnitude as our estimate of the observed amplitude, which gives best-fitting values $\phi = 60$ for the combined model and $\phi = 100$ for the host–pathogen model. In Fig. 3, however, we use $\phi = 20$ to illustrate the origins of complex dynamics.

In calculating the statistics in Table 1, we restricted ourselves to time series with at least five outbreaks, to reduce the uncertainty in our estimates of the coefficient of variation of the time between outbreaks. Also, to illustrate irregularity in the inter-outbreak period, we used only species for which the coefficient of variation of the time between outbreaks was at least 0.15. In the case of the gypsy moth (*Lymantria dispar*) and the Douglas-fir tussock moth (*Orgyia pseudotsugata*) the data are spatially referenced. Because the model assumes that populations are well-mixed—so that dispersal does not limit species interactions—for the gypsy moth we used data for particular states, while for the tussock moth we used outbreak regions as in the original source[16]. At these scales, populations are nearly synchronous[27]. Data were periods of outbreaks, except for the following. *Lymantria dispar* data were acres defoliated, and outbreaks were defined as periods in which the area defoliated was more than 1,000 acres, a common definition of an outbreak for defoliation data. *Bupalus piniarius* data were densities, and outbreaks were defined as periods during which the insect's density was greater than its mean density.

Received 10 December 2003; accepted 13 April 2004; doi:10.1038/nature02569.

1. Myers, J. H. Can a general hypothesis explain population cycles of forest Lepidoptera? *Adv. Ecol. Res.* **18,** 179–242 (1988).
2. Liebhold, A. & Kamata, N. Are population cycles and spatial synchrony a universal characteristic of forest insect populations? *Popul. Ecol.* **42,** 205–209 (2000).
3. Varley, G. C., Gradwell, G. R. & Hassell, M. P. *Insect Population Ecology: An Analytical Approach* 135–153 (Blackwell Scientific, Oxford, 1973).
4. Anderson, R. M. & May, R. M. The population-dynamics of micro-parasites and their invertebrate hosts. *Phil. Trans. R. Soc. Lond. B* **291,** 451–524 (1981).
5. Mason, R. R., Torgerson, T. R., Wickman, B. E. & Paul, H. G. Natural regulation of a Douglas-fir tussock moth (Lepidoptera: Lymantriidae) population in the Sierra Nevada. *Environ. Entomol.* **12,** 587–594 (1983).
6. Elkinton, J. S. *et al.* Interactions among gypsy moths, white-footed mice, and acorns. *Ecology* **77,** 2332–2342 (1996).
7. Parry, D., Spence, J. R. & Volney, W. J. A. Response of natural enemies to experimentally increased populations of the forest tent caterpillar, *Malacosoma disstria*. *Ecol. Entomol.* **22,** 97–108 (1997).
8. Klemola, T., Tanhuanpää, M., Korpimäki, E. & Ruohomäki, K. Specialist and generalist natural enemies as an explanation for geographical gradients in population cycles of northern herbivores. *Oikos* **99,** 83–94 (2002).
9. Southwood, T. R. E. & Comins, H. N. A synoptic population model. *J. Anim. Ecol.* **45,** 949–965 (1976).
10. May, R. M. Thresholds and breakpoints in ecosystems with a multiplicity of stable states. *Nature* **269,** 471–477 (1977).
11. Ludwig, D., Jones, D. D. & Holling, C. S. Qualitative analysis of insect outbreak systems: the spruce budworm and forest. *J. Anim. Ecol.* **47,** 315–332 (1978).
12. Rand, D. & Wilson, H. B. Chaotic stochasticity: a ubiquitous source of unpredictability in epidemics. *Proc. R. Soc. Lond. B* **246,** 179–184 (1991).
13. Dennis, B., Desharnais, R. A., Cushing, J. M., Henson, S. M. & Constantino, R. F. Estimating chaos and complex dynamics in an insect population. *Ecol. Monogr.* **71,** 277–303 (2001).
14. Cory, J. S., Hails, R. S. & Sait, S. M. in *The Baculoviruses* (ed. Miller, L. K.) 301–339 (Plenum, New York, 1997).
15. Woods, S. & Elkinton, J. S. Bimodal patterns of mortality from nuclear polyhedrosis virus in gypsy moth (*Lymantria dispar*) populations. *J. Invertebr. Pathol.* **50,** 151–157 (1987).
16. Shepherd, R. F. Evidence of synchronized cycles in outbreak patterns of Douglas-fir tussock moth, *Orgyia pseudotsugata* (McDunnough) (Lepidoptera: Lymantriidae). *Mem. Entomol. Soc. Can.* **146,** 107–121 (1988).
17. Murray, K. D. & Elkinton, J. S. Environmental contamination of egg masses as a major component of transgenerational transmission of gypsy-moth nuclear polyhedrosis virus (LdMNPV). *J. Invertebr. Pathol.* **53,** 324–334 (1989).
18. Dwyer, G., Elkinton, J. S. & Buonaccorsi, J. P. Host heterogeneity in susceptibility and disease dynamics: tests of a mathematical model. *Am. Nat.* **150,** 685–707 (1997).
19. Dwyer, G., Dushoff, J., Elkinton, J. S. & Levin, S. A. Pathogen-driven outbreaks in forest defoliators revisited: building models from experimental data. *Am. Nat.* **156,** 105–120 (2000).
20. Hunter, A. F. in *Population Dynamics: New Approaches and Synthesis* (eds Cappuccino, N. & Price, P. W.) 41–64 (Academic, New York, 1995).
21. Gould, J. R., Elkinton, J. S. & Wallner, W. E. Density-dependent suppression of experimentally created gypsy moth *Lymantria dispar* (Lepidoptera: Lymantriidae) populations by natural enemies. *J. Anim. Ecol.* **59,** 213–233 (1990).
22. Holling, C. S. Some characteristics of simple types of predation and parasitism. *Can. Entomol.* **91,** 293–320 (1959).
23. Kendall, B. E. *et al.* Why do populations cycle? A synthesis of statistical and mechanistic modeling approaches. *Ecology* **80,** 1789–1805 (1999).
24. Bjornstad, O. N. Cycles and synchrony: two historical experiments and one 'experience'. *J. Anim. Ecol.* **69,** 869–873 (2000).
25. Scheffer, S., Carpenter, S., Foley, J. A., Folkes, C. & Walker, B. Catastrophic shifts in ecosystems. *Nature* **413,** 591–596 (2001).
26. Williams, D. W. *et al.* Oak defoliation and population density relationships for the Gypsy Moth (Lepidoptera: Lymantriidae). *J. Econ. Entomol.* **84,** 1508–1514 (1991).
27. Williams, D. W. & Liebhold, A. M. Influence of weather on the synchrony of gypsy moth (Lepidoptera: Lymantriidae) outbreaks in New England. *Environ. Entomol.* **24,** 987–995 (1995).
28. Schwerdtfeger, R. Über die ursachen des massenwechsels der insekten. *Z. Angew. Entomol.* **28,** 254–303 (1941).
29. Ruohomäki, K. *et al.* Causes of cyclicity of *Epirrita autumnata* (Lepidoptera, Geometridae): grandiose theory and tedious practice. *Popul. Ecol.* **42,** 211–223 (2000).
30. Liebhold, A., Kamata, N. & Jacobs, T. Cyclicity and synchrony of historical outbreaks of the beech caterpillar, *Quadricalcarifera punctatella* (Motschulsky) in Japan. *Res. Popul. Ecol.* **38,** 87–94 (1996).

Supplementary Information accompanies the paper on **www.nature.com/nature**.

Acknowledgements We thank O. Bjornstad, P. Turchin and A. Hunter for comments. G.D. and J.D. were supported by grants from the US National Science Foundation. J.D. was also supported by the Andrew W. Mellon Foundation.

Competing interests statement The authors declare that they have no competing financial interests.

Correspondence and requests for materials should be addressed to G.D. (gdwyer@uchicago.edu).

An SCF-like ubiquitin ligase complex that controls presynaptic differentiation

Edward H. Liao[1], Wesley Hung[1], Benjamin Abrams[2] & Mei Zhen[1]

[1]*Department of Medical Genetics and Microbiology, Samuel Lunenfeld Research Institute, University of Toronto, Ontario, Canada M5G 1X5*
[2]*Department of Molecular, Cell and Developmental Biology, University of California, Santa Cruz, California 95064, USA*

During synapse formation, specialized subcellular structures develop at synaptic junctions in a tightly regulated fashion. Cross-signalling initiated by ephrins, Wnts and transforming growth factor-β family members between presynaptic and post-synaptic termini are proposed to govern synapse formation[1–3]. It is not well understood how multiple signals are integrated and regulated by developing synaptic termini to control synaptic differentiation. Here we report the identification of FSN-1, a novel F-box protein that is required in presynaptic neurons for the restriction and/or maturation of synapses in *Caenorhabditis elegans*. Many F-box proteins are target recognition subunits of SCF (Skp, Cullin, F-box) ubiquitin-ligase complexes[4–7]. *fsn-1* functions in the same pathway as *rpm-1*, a gene encoding a large protein with RING finger domains[8,9]. FSN-1 physically associates with RPM-1 and the *C. elegans* homologues of SKP1 and Cullin to form a new type of SCF complex at presynaptic periactive zones. We provide evidence that T10H9.2, which encodes the *C. elegans* receptor tyrosine kinase ALK (anaplastic lymphoma kinase[10]), may be a target or a downstream effector through which FSN-1 stabilizes synapse formation. This neuron-specific, SCF-like complex therefore provides a localized signal to attenuate presynaptic differentiation.

Drosophila and *C. elegans* provide genetic models for uncovering conserved regulatory mechanisms for synapse differentiation[11,12].